

A coupled-channel analysis of the $X(3872)$ lineshape with BESIII data

M. Ablikim¹, M. N. Achasov^{5,b}, P. Adlarson⁷⁵, X. C. Ai⁸¹, R. Aliberti³⁶, A. Amoroso^{74A,74C}, M. R. An⁴⁰, Q. An^{71,58}, Y. Bai⁵⁷, O. Bakina³⁷, I. Balossino^{30A}, Y. Ban^{47,g}, V. Batozskaya^{1,45}, K. Begzsuren³³, N. Berger³⁶, M. Berlowski⁴⁵, M. Bertani^{29A}, D. Bettoni^{30A}, F. Bianchi^{74A,74C}, E. Bianco^{74A,74C}, A. Bortone^{74A,74C}, I. Boyko³⁷, R. A. Briere⁶, A. Brueggemann⁶⁸, H. Cai⁷⁶, X. Cai^{1,58}, A. Calcaterra^{29A}, G. F. Cao^{1,63}, N. Cao^{1,63}, S. A. Cetin^{62A}, J. F. Chang^{1,58}, T. T. Chang⁷⁷, W. L. Chang^{1,63}, G. R. Che⁴⁴, G. Chelkov^{37,a}, C. Chen⁴⁴, Chao Chen⁵⁵, G. Chen¹, H. S. Chen^{1,63}, M. L. Chen^{1,58,63}, S. J. Chen⁴³, S. M. Chen⁶¹, T. Chen^{1,63}, X. R. Chen^{32,63}, X. T. Chen^{1,63}, Y. B. Chen^{1,58}, Y. Q. Chen³⁵, Z. J. Chen^{26,h}, W. S. Cheng^{74C}, S. K. Choi^{11A}, X. Chu⁴⁴, G. Cibinetto^{30A}, S. C. Coen⁴, F. Cossio^{74C}, J. J. Cui⁵⁰, H. L. Dai^{1,58}, J. P. Dai⁷⁹, A. Dbeyssi¹⁹, R. E. de Boer⁴, D. Dedovich³⁷, Z. Y. Deng¹, A. Denig³⁶, I. Denysenko³⁷, M. Destefanis^{74A,74C}, F. De Mori^{74A,74C}, B. Ding^{66,1}, X. X. Ding^{47,g}, Y. Ding⁴¹, Y. Ding³⁵, J. Dong^{1,58}, L. Y. Dong^{1,63}, M. Y. Dong^{1,58,63}, X. Dong⁷⁶, M. C. Du¹, S. X. Du⁸¹, Z. H. Duan⁴³, P. Egorov^{37,a}, Y. L. Fan⁷⁶, J. Fang^{1,58}, S. S. Fang^{1,63}, W. X. Fang¹, Y. Fang¹, R. Farinelli^{30A}, L. Fava^{74B,74C}, F. Feldbauer⁴, G. Felici^{29A}, C. Q. Feng^{71,58}, J. H. Feng⁵⁹, K. Fischer⁶⁹, M. Fritsch⁴, C. Fritsch⁶⁸, C. D. Fu¹, J. L. Fu⁶³, Y. W. Fu¹, H. Gao⁶³, Y. N. Gao^{47,g}, Yang Gao^{71,58}, S. Garbolino^{74C}, I. Garzia^{30A,30B}, P. T. Ge⁷⁶, Z. W. Ge⁴³, C. Geng⁵⁹, E. M. Gersabeck⁶⁷, A. Gilman⁶⁹, K. Goetzen¹⁴, L. Gong⁴¹, W. X. Gong^{1,58}, W. Gradl³⁶, S. Gramigna^{30A,30B}, M. Greco^{74A,74C}, M. H. Gu^{1,58}, Y. T. Gu¹⁶, C. Y. Guan^{1,63}, Z. L. Guan²³, A. Q. Guo^{32,63}, L. B. Guo⁴², M. J. Guo⁵⁰, R. P. Guo⁴⁹, Y. P. Guo^{13,f}, A. Guskov^{37,a}, T. T. Han⁵⁰, W. Y. Han⁴⁰, X. Q. Hao²⁰, F. A. Harris⁶⁵, K. K. He⁵⁵, K. L. He^{1,63}, F. H. Heinsius⁴, C. H. Heinz³⁶, Y. K. Heng^{1,58,63}, C. Herold⁶⁰, T. Holtmann⁴, P. C. Hong^{13,f}, G. Y. Hou^{1,63}, X. T. Hou^{1,63}, Y. R. Hou⁶³, Z. L. Hou¹, H. M. Hu^{1,63}, J. F. Hu^{56,i}, T. Hu^{1,58,63}, Y. Hu¹, G. S. Huang^{71,58}, K. X. Huang⁵⁹, L. Q. Huang^{32,63}, X. T. Huang⁵⁰, Y. P. Huang¹, T. Hussain⁷³, N. Hüskens^{28,36}, W. Imoehl²⁸, M. Irshad^{71,58}, J. Jackson²⁸, S. Jaeger⁴, S. Janchiv³³, J. H. Jeong^{11A}, Q. Ji¹, Q. P. Ji²⁰, X. B. Ji^{1,63}, X. L. Ji^{1,58}, Y. Y. Ji⁵⁰, X. Q. Jia⁵⁰, Z. K. Jia^{71,58}, H. J. Jiang⁷⁶, P. C. Jiang^{47,g}, S. S. Jiang⁴⁰, T. J. Jiang¹⁷, X. S. Jiang^{1,58,63}, Y. Jiang⁶³, J. B. Jiao⁵⁰, Z. Jiao²⁴, S. Jin⁴³, Y. Jin⁶⁶, M. Q. Jing^{1,63}, T. Johansson⁷⁵, X. K.¹, S. Kabana³⁴, N. Kalantar-Nayestanaki⁶⁴, X. L. Kang¹⁰, X. S. Kang⁴¹, R. Kappert⁶⁴, M. Kavatsyuk⁶⁴, B. C. Ke⁸¹, A. Khoukaz⁶⁸, R. Kiuchi¹, R. Kliemt¹⁴, O. B. Kolcu^{62A}, B. Kopf⁴, M. Kuessner⁴, A. Kupsc^{45,75}, W. Kühn³⁸, J. J. Lane⁶⁷, P. Larin¹⁹, A. Lavania²⁷, L. Lavezzi^{74A,74C}, T. T. Lei^{71,k}, Z. H. Lei^{71,58}, H. Leithoff³⁶, M. Lellmann³⁶, T. Lenz³⁶, C. Li⁴⁸, C. Li⁴⁴, C. H. Li⁴⁰, Cheng Li^{71,58}, D. M. Li⁸¹, F. Li^{1,58}, G. Li¹, H. Li^{71,58}, H. B. Li^{1,63}, H. J. Li²⁰, H. N. Li^{56,i}, Hui Li⁴⁴, J. R. Li⁶¹, J. S. Li⁵⁹, J. W. Li⁵⁰, K. L. Li²⁰, Ke Li¹, L. J. Li^{1,63}, L. K. Li¹, Lei Li³, M. H. Li⁴⁴, P. R. Li^{39,j,k}, Q. X. Li⁵⁰, S. X. Li¹³, T. Li⁵⁰, W. D. Li^{1,63}, W. G. Li¹, X. H. Li^{71,58}, X. L. Li⁵⁰, Xiaoyu Li^{1,63}, Y. G. Li^{47,g}, Z. J. Li⁵⁹, Z. X. Li¹⁶, C. Liang⁴³, H. Liang^{1,63}, H. Liang^{71,58}, H. Liang³⁵, Y. F. Liang⁵⁴, Y. T. Liang^{32,63}, G. R. Liao¹⁵, L. Z. Liao⁵⁰, Y. P. Liao^{1,63}, J. Libby²⁷, A. Limphirat⁶⁰, D. X. Lin^{32,63}, T. Lin¹, B. J. Liu¹, B. X. Liu⁷⁶, C. Liu³⁵, C. X. Liu¹, F. H. Liu⁵³, Fang Liu¹, Feng Liu⁷, G. M. Liu^{56,i}, H. Liu^{39,j,k}, H. B. Liu¹⁶, H. M. Liu^{1,63}, Huanhuan Liu¹, Huihui Liu²², J. B. Liu^{71,58}, J. L. Liu⁷², J. Y. Liu^{1,63}, K. Liu¹, K. Y. Liu⁴¹, Ke Liu²³, L. Liu^{71,58}, L. C. Liu⁴⁴, Lu Liu⁴⁴, M. H. Liu^{13,f}, P. L. Liu¹, Q. Liu⁶³, S. B. Liu^{71,58}, T. Liu^{13,f}, W. K. Liu⁴⁴, W. M. Liu^{71,58}, X. Liu^{39,j,k}, Y. Liu⁸¹, Y. Liu^{39,j,k}, Y. B. Liu⁴⁴, Z. A. Liu^{1,58,63}, Z. Q. Liu⁵⁰, X. C. Lou^{1,58,63}, F. X. Lu⁵⁹, H. J. Lu²⁴, J. G. Lu^{1,58}, X. L. Lu¹, Y. Lu⁸, Y. P. Lu^{1,58}, Z. H. Lu^{1,63}, C. L. Luo⁴², M. X. Luo⁸⁰, T. Luo^{13,f}, X. L. Luo^{1,58}, X. R. Lyu⁶³, Y. F. Lyu⁴⁴, F. C. Ma⁴¹, H. L. Ma¹, J. L. Ma^{1,63}, L. L. Ma⁵⁰, M. M. Ma^{1,63}, Q. M. Ma¹, R. Q. Ma^{1,63}, R. T. Ma⁶³, X. Y. Ma^{1,58}, Y. Ma^{47,g}, Y. M. Ma³², F. E. Maas¹⁹, M. Maggiora^{74A,74C}, S. Malde⁶⁹, Q. A. Malik⁷³, A. Mangoni^{29B}, Y. J. Mao^{47,g}, Z. P. Mao¹, S. Marcello^{74A,74C}, Z. X. Meng⁶⁶, J. G. Messchendorp^{14,64}, G. Mezzadri^{30A}, H. Miao^{1,63}, T. J. Min⁴³, R. E. Mitchell²⁸, X. H. Mo^{1,58,63}, N. Yu. Muchnoi^{5,b}, Y. Nefedov³⁷, F. Nerling^{19,d}, I. B. Nikolaev^{5,b}, Z. Ning^{1,58}, S. Nisar^{12,l}, Y. Niu⁵⁰, S. L. Olsen⁶³, Q. Ouyang^{1,58,63}, S. Pacetti^{29B,29C}, X. Pan⁵⁵, Y. Pan⁵⁷, A. Pathak³⁵, P. Patteri^{29A}, Y. P. Pei^{71,58}, M. Pelizaeus⁴, H. P. Peng^{71,58}, K. Peters^{14,d}, J. L. Ping⁴², R. G. Ping^{1,63}, S. Plura³⁶, S. Pogodin³⁷, V. Prasad³⁴, F. Z. Qi¹, H. Qi^{71,58}, H. R. Qi⁶¹, M. Qi⁴³, T. Y. Qi^{13,f}, S. Qian^{1,58}, W. B. Qian⁶³, C. F. Qiao⁶³, J. J. Qin⁷², L. Q. Qin¹⁵, X. P. Qin^{13,f}, X. S. Qin⁵⁰, Z. H. Qin^{1,58}, J. F. Qiu¹, S. Q. Qu⁶¹, C. F. Redmer³⁶, K. J. Ren⁴⁰, A. Rivetti^{74C}, V. Rodin⁶⁴, M. Rolo^{74C}, G. Rong^{1,63}, Ch. Rosner¹⁹, S. N. Ruan⁴⁴, N. Salone⁴⁵, A. Sarantsev^{37,c}, Y. Schelhaas³⁶, K. Schoenning⁷⁵, M. Scodreggio^{30A,30B}, K. Y. Shan^{13,f}, W. Shan²⁵, X. Y. Shan^{71,58}, J. F. Shangguan⁵⁵, L. G. Shao^{1,63}, M. Shao^{71,58}, C. P. Shen^{13,f}, H. F. Shen^{1,63}, W. H. Shen⁶³, X. Y. Shen^{1,63}, B. A. Shi⁶³, H. C. Shi^{71,58}, J. L. Shi¹³, J. Y. Shi¹, Q. Q. Shi⁵⁵, R. S. Shi^{1,63}, X. Shi^{1,58}, J. J. Song²⁰, T. Z. Song⁵⁹, W. M. Song^{35,1}, Y. J. Song¹³, Y. X. Song^{47,g}, S. Sosio^{74A,74C}, S. Spataro^{74A,74C}, F. Stieler³⁶, Y. J. Su⁶³, G. B. Sun⁷⁶, G. X. Sun¹, H. Sun⁶³, H. K. Sun¹, J. F. Sun²⁰, K. Sun⁶¹, L. Sun⁷⁶, S. S. Sun^{1,63}, T. Sun^{1,63}, W. Y. Sun³⁵, Y. Sun¹⁰, Y. J. Sun^{71,58}, Y. Z. Sun¹, Z. T. Sun⁵⁰, Y. X. Tan^{71,58}, C. J. Tang⁵⁴, G. Y. Tang¹, J. Tang⁵⁹, Y. A. Tang⁷⁶, L. Y. Tao⁷², Q. T. Tao^{26,h}, M. Tat⁶⁹, J. X. Teng^{71,58}, V. Thoren⁷⁵, W. H. Tian⁵², W. H. Tian⁵⁹,

Y. Tian^{32,63}, Z. F. Tian⁷⁶, I. Uman^{62B}, S. J. Wang⁵⁰, B. Wang¹, B. L. Wang⁶³, Bo Wang^{71,58}, C. W. Wang⁴³,
 D. Y. Wang^{47,9}, F. Wang⁷², H. J. Wang^{39,j,k}, H. P. Wang^{1,63}, J. P. Wang⁵⁰, K. Wang^{1,58}, L. L. Wang¹,
 M. Wang⁵⁰, Meng Wang^{1,63}, S. Wang^{13,f}, S. Wang^{39,j,k}, T. Wang^{13,f}, T. J. Wang⁴⁴, W. Wang⁷², W. Wang⁵⁹,
 W. P. Wang^{71,58}, X. Wang^{47,g}, X. F. Wang^{39,j,k}, X. J. Wang⁴⁰, X. L. Wang^{13,f}, Y. Wang⁶¹, Y. D. Wang⁴⁶,
 Y. F. Wang^{1,58,63}, Y. H. Wang⁴⁸, Y. N. Wang⁴⁶, Y. Q. Wang¹, Yaqian Wang^{18,1}, Yi Wang⁶¹, Z. Wang^{1,58}, Z. L.
 Wang⁷², Z. Y. Wang^{1,63}, Ziyi Wang⁶³, D. Wei⁷⁰, D. H. Wei¹⁵, F. Weidner⁶⁸, S. P. Wen¹, C. W. Wenzel⁴,
 U. Wiedner⁴, G. Wilkinson⁶⁹, M. Wolke⁷⁵, L. Wollenberg⁴, C. Wu⁴⁰, J. F. Wu^{1,63}, L. H. Wu¹, L. J. Wu^{1,63},
 X. Wu^{13,f}, X. H. Wu³⁵, Y. Wu⁷¹, Y. J. Wu³², Z. Wu^{1,58}, L. Xia^{71,58}, X. M. Xian⁴⁰, T. Xiang^{47,g}, D. Xiao^{39,j,k},
 G. Y. Xiao⁴³, S. Y. Xiao¹, Y. L. Xiao^{13,f}, Z. J. Xiao⁴², C. Xie⁴³, X. H. Xie^{47,g}, Y. Xie⁵⁰, Y. G. Xie^{1,58}, Y. H. Xie⁷,
 Z. P. Xie^{71,58}, T. Y. Xing^{1,63}, C. F. Xu^{1,63}, C. J. Xu⁵⁹, G. F. Xu¹, H. Y. Xu⁶⁶, Q. J. Xu¹⁷, Q. N. Xu³¹, W. Xu^{1,63},
 W. L. Xu⁶⁶, X. P. Xu⁵⁵, Y. C. Xu⁷⁸, Z. P. Xu⁴³, Z. S. Xu⁶³, F. Yan^{13,f}, L. Yan^{13,f}, W. B. Yan^{71,58}, W. C. Yan⁸¹,
 X. Q. Yan¹, H. J. Yang^{51,e}, H. L. Yang³⁵, H. X. Yang¹, Tao Yang¹, Y. Yang^{13,f}, Y. F. Yang⁴⁴, Y. X. Yang^{1,63},
 Yifan Yang^{1,63}, Z. W. Yang^{39,j,k}, Z. P. Yao⁵⁰, M. Ye^{1,58}, M. H. Ye⁹, J. H. Yin¹, Z. Y. You⁵⁹, B. X. Yu^{1,58,63},
 C. X. Yu⁴⁴, G. Yu^{1,63}, J. S. Yu^{26,h}, T. Yu⁷², X. D. Yu^{47,g}, C. Z. Yuan^{1,63}, L. Yuan², S. C. Yuan¹, X. Q. Yuan¹,
 Y. Yuan^{1,63}, Z. Y. Yuan⁵⁹, C. X. Yue⁴⁰, A. A. Zafar⁷³, F. R. Zeng⁵⁰, X. Zeng^{13,f}, Y. Zeng^{26,h}, Y. J. Zeng^{1,63},
 X. Y. Zhai³⁵, Y. C. Zhai⁵⁰, Y. H. Zhan⁵⁹, A. Q. Zhang^{1,63}, B. L. Zhang^{1,63}, B. X. Zhang¹, D. H. Zhang⁴⁴,
 G. Y. Zhang²⁰, H. Zhang⁷¹, H. H. Zhang⁵⁹, H. H. Zhang³⁵, H. Q. Zhang^{1,58,63}, H. Y. Zhang^{1,58}, J. J. Zhang⁵²,
 J. L. Zhang²¹, J. Q. Zhang⁴², J. W. Zhang^{1,58,63}, J. X. Zhang^{39,j,k}, J. Y. Zhang¹, J. Z. Zhang^{1,63}, Jianyu Zhang⁶³,
 Jiawei Zhang^{1,63}, L. M. Zhang⁶¹, L. Q. Zhang⁵⁹, Lei Zhang⁴³, P. Zhang¹, Q. Y. Zhang^{40,81}, Shuihan Zhang^{1,63},
 Shulei Zhang^{26,h}, X. D. Zhang⁴⁶, X. M. Zhang¹, X. Y. Zhang⁵⁰, Xuyan Zhang⁵⁵, Y. Zhang⁷², Y. Zhang⁶⁹, Y.
 T. Zhang⁸¹, Y. H. Zhang^{1,58}, Yan Zhang^{71,58}, Yao Zhang¹, Z. H. Zhang¹, Z. L. Zhang³⁵, Z. Y. Zhang⁴⁴,
 Z. Y. Zhang⁷⁶, G. Zhao¹, J. Zhao⁴⁰, J. Y. Zhao^{1,63}, J. Z. Zhao^{1,58}, Lei Zhao^{71,58}, Ling Zhao¹, M. G. Zhao⁴⁴,
 S. J. Zhao⁸¹, Y. B. Zhao^{1,58}, Y. X. Zhao^{32,63}, Z. G. Zhao^{71,58}, A. Zhemchugov^{37,a}, B. Zheng⁷², J. P. Zheng^{1,58},
 W. J. Zheng^{1,63}, Y. H. Zheng⁶³, B. Zhong⁴², X. Zhong⁵⁹, H. Zhou⁵⁰, L. P. Zhou^{1,63}, X. Zhou⁷⁶, X. K. Zhou⁷,
 X. R. Zhou^{71,58}, X. Y. Zhou⁴⁰, Y. Z. Zhou^{13,f}, J. Zhu⁴⁴, K. Zhu¹, K. J. Zhu^{1,58,63}, L. Zhu³⁵, L. X. Zhu⁶³,
 S. H. Zhu⁷⁰, S. Q. Zhu⁴³, T. J. Zhu^{13,f}, W. J. Zhu^{13,f}, Y. C. Zhu^{71,58}, Z. A. Zhu^{1,63}, J. H. Zou¹, J. Zu^{71,58}

(BESIII Collaboration)

¹ *Institute of High Energy Physics, Beijing 100049, People's Republic of China*

² *Beihang University, Beijing 100191, People's Republic of China*

³ *Beijing Institute of Petrochemical Technology, Beijing 102617, People's Republic of China*

⁴ *Bochum Ruhr-University, D-44780 Bochum, Germany*

⁵ *Budker Institute of Nuclear Physics SB RAS (BINP), Novosibirsk 630090, Russia*

⁶ *Carnegie Mellon University, Pittsburgh, Pennsylvania 15213, USA*

⁷ *Central China Normal University, Wuhan 430079, People's Republic of China*

⁸ *Central South University, Changsha 410083, People's Republic of China*

⁹ *China Center of Advanced Science and Technology, Beijing 100190, People's Republic of China*

¹⁰ *China University of Geosciences, Wuhan 430074, People's Republic of China*

¹¹ *Chung-Ang University, Seoul, 06974, Republic of Korea*

¹² *COMSATS University Islamabad, Lahore Campus, Defence Road, Off Raiwind Road, 54000 Lahore, Pakistan*

¹³ *Fudan University, Shanghai 200433, People's Republic of China*

¹⁴ *GSI Helmholtzcentre for Heavy Ion Research GmbH, D-64291 Darmstadt, Germany*

¹⁵ *Guangxi Normal University, Guilin 541004, People's Republic of China*

¹⁶ *Guangxi University, Nanning 530004, People's Republic of China*

¹⁷ *Hangzhou Normal University, Hangzhou 310036, People's Republic of China*

¹⁸ *Hebei University, Baoding 071002, People's Republic of China*

¹⁹ *Helmholtz Institute Mainz, Staudinger Weg 18, D-55099 Mainz, Germany*

²⁰ *Henan Normal University, Xinxiang 453007, People's Republic of China*

²¹ *Henan University, Kaifeng 475004, People's Republic of China*

²² *Henan University of Science and Technology, Luoyang 471003, People's Republic of China*

²³ *Henan University of Technology, Zhengzhou 450001, People's Republic of China*

²⁴ *Huangshan College, Huangshan 245000, People's Republic of China*

²⁵ *Hunan Normal University, Changsha 410081, People's Republic of China*

²⁶ *Hunan University, Changsha 410082, People's Republic of China*

- ²⁷ Indian Institute of Technology Madras, Chennai 600036, India
- ²⁸ Indiana University, Bloomington, Indiana 47405, USA
- ²⁹ INFN Laboratori Nazionali di Frascati , (A)INFN Laboratori Nazionali di Frascati, I-00044, Frascati, Italy; (B)INFN Sezione di Perugia, I-06100, Perugia, Italy; (C)University of Perugia, I-06100, Perugia, Italy
- ³⁰ INFN Sezione di Ferrara, (A)INFN Sezione di Ferrara, I-44122, Ferrara, Italy; (B)University of Ferrara, I-44122, Ferrara, Italy
- ³¹ Inner Mongolia University, Hohhot 010021, People's Republic of China
- ³² Institute of Modern Physics, Lanzhou 730000, People's Republic of China
- ³³ Institute of Physics and Technology, Peace Avenue 54B, Ulaanbaatar 13330, Mongolia
- ³⁴ Instituto de Alta Investigación, Universidad de Tarapacá, Casilla 7D, Arica 1000000, Chile
- ³⁵ Jilin University, Changchun 130012, People's Republic of China
- ³⁶ Johannes Gutenberg University of Mainz, Johann-Joachim-Becher-Weg 45, D-55099 Mainz, Germany
- ³⁷ Joint Institute for Nuclear Research, 141980 Dubna, Moscow region, Russia
- ³⁸ Justus-Liebig-Universitaet Giessen, II. Physikalisches Institut, Heinrich-Buff-Ring 16, D-35392 Giessen, Germany
- ³⁹ Lanzhou University, Lanzhou 730000, People's Republic of China
- ⁴⁰ Liaoning Normal University, Dalian 116029, People's Republic of China
- ⁴¹ Liaoning University, Shenyang 110036, People's Republic of China
- ⁴² Nanjing Normal University, Nanjing 210023, People's Republic of China
- ⁴³ Nanjing University, Nanjing 210093, People's Republic of China
- ⁴⁴ Nankai University, Tianjin 300071, People's Republic of China
- ⁴⁵ National Centre for Nuclear Research, Warsaw 02-093, Poland
- ⁴⁶ North China Electric Power University, Beijing 102206, People's Republic of China
- ⁴⁷ Peking University, Beijing 100871, People's Republic of China
- ⁴⁸ Qufu Normal University, Qufu 273165, People's Republic of China
- ⁴⁹ Shandong Normal University, Jinan 250014, People's Republic of China
- ⁵⁰ Shandong University, Jinan 250100, People's Republic of China
- ⁵¹ Shanghai Jiao Tong University, Shanghai 200240, People's Republic of China
- ⁵² Shanxi Normal University, Linfen 041004, People's Republic of China
- ⁵³ Shanxi University, Taiyuan 030006, People's Republic of China
- ⁵⁴ Sichuan University, Chengdu 610064, People's Republic of China
- ⁵⁵ Soochow University, Suzhou 215006, People's Republic of China
- ⁵⁶ South China Normal University, Guangzhou 510006, People's Republic of China
- ⁵⁷ Southeast University, Nanjing 211100, People's Republic of China
- ⁵⁸ State Key Laboratory of Particle Detection and Electronics, Beijing 100049, Hefei 230026, People's Republic of China
- ⁵⁹ Sun Yat-Sen University, Guangzhou 510275, People's Republic of China
- ⁶⁰ Suranaree University of Technology, University Avenue 111, Nakhon Ratchasima 30000, Thailand
- ⁶¹ Tsinghua University, Beijing 100084, People's Republic of China
- ⁶² Turkish Accelerator Center Particle Factory Group, (A)Istinye University, 34010, Istanbul, Turkey; (B)Near East University, Nicosia, North Cyprus, 99138, Mersin 10, Turkey
- ⁶³ University of Chinese Academy of Sciences, Beijing 100049, People's Republic of China
- ⁶⁴ University of Groningen, NL-9747 AA Groningen, The Netherlands
- ⁶⁵ University of Hawaii, Honolulu, Hawaii 96822, USA
- ⁶⁶ University of Jinan, Jinan 250022, People's Republic of China
- ⁶⁷ University of Manchester, Oxford Road, Manchester, M13 9PL, United Kingdom
- ⁶⁸ University of Muenster, Wilhelm-Klemm-Strasse 9, 48149 Muenster, Germany
- ⁶⁹ University of Oxford, Keble Road, Oxford OX13RH, United Kingdom
- ⁷⁰ University of Science and Technology Liaoning, Anshan 114051, People's Republic of China
- ⁷¹ University of Science and Technology of China, Hefei 230026, People's Republic of China
- ⁷² University of South China, Hengyang 421001, People's Republic of China
- ⁷³ University of the Punjab, Lahore-54590, Pakistan
- ⁷⁴ University of Turin and INFN, (A)University of Turin, I-10125, Turin, Italy; (B)University of Eastern Piedmont, I-15121, Alessandria, Italy; (C)INFN, I-10125, Turin, Italy

⁷⁵ Uppsala University, Box 516, SE-75120 Uppsala, Sweden

⁷⁶ Wuhan University, Wuhan 430072, People's Republic of China

⁷⁷ Xinyang Normal University, Xinyang 464000, People's Republic of China

⁷⁸ Yantai University, Yantai 264005, People's Republic of China

⁷⁹ Yunnan University, Kunming 650500, People's Republic of China

⁸⁰ Zhejiang University, Hangzhou 310027, People's Republic of China

⁸¹ Zhengzhou University, Zhengzhou 450001, People's Republic of China

^a Also at the Moscow Institute of Physics and Technology, Moscow 141700, Russia

^b Also at the Novosibirsk State University, Novosibirsk, 630090, Russia

^c Also at the NRC "Kurchatov Institute", PNPI, 188300, Gatchina, Russia

^d Also at Goethe University Frankfurt, 60323 Frankfurt am Main, Germany

^e Also at Key Laboratory for Particle Physics, Astrophysics and Cosmology, Ministry of Education; Shanghai Key Laboratory for Particle Physics and Cosmology; Institute of Nuclear and Particle Physics, Shanghai 200240, People's Republic of China

^f Also at Key Laboratory of Nuclear Physics and Ion-beam Application (MOE) and Institute of Modern Physics, Fudan University, Shanghai 200443, People's Republic of China

^g Also at State Key Laboratory of Nuclear Physics and Technology, Peking University, Beijing 100871, People's Republic of China

^h Also at School of Physics and Electronics, Hunan University, Changsha 410082, China

ⁱ Also at Guangdong Provincial Key Laboratory of Nuclear Science, Institute of Quantum Matter, South China Normal University, Guangzhou 510006, China

^j Also at Frontiers Science Center for Rare Isotopes, Lanzhou University, Lanzhou 730000, People's Republic of China

^k Also at Lanzhou Center for Theoretical Physics, Lanzhou University, Lanzhou 730000, People's Republic of China

^l Also at the Department of Mathematical Sciences, IBA, Karachi 75270, Pakistan

(Dated: September 6, 2023)

We perform a study of the $X(3872)$ lineshape using the data samples of $e^+e^- \rightarrow \gamma X(3872)$, $X(3872) \rightarrow D^0 \bar{D}^0 \pi^0$ and $\pi^+ \pi^- J/\psi$ collected with the BESIII detector. The effects of the coupled-channels and the off-shell D^{*0} are included in the parameterization of the lineshape. The lineshape mass parameter is obtained to be $M_X = (3871.63 \pm 0.13_{-0.05}^{+0.06})$ MeV. Two poles are found on the first and second Riemann sheets corresponding to the $D^{*0} \bar{D}^0$ branch cut. The pole location on the first sheet is much closer to the $D^{*0} \bar{D}^0$ threshold than the other, and is determined to be $7.04 \pm 0.15_{-0.08}^{+0.07}$ MeV above the $D^0 \bar{D}^0 \pi^0$ threshold with an imaginary part $-0.19 \pm 0.08_{-0.19}^{+0.14}$ MeV.

The $X(3872)$ was discovered in $B^\pm \rightarrow [X(3872) \rightarrow \pi^+ \pi^- J/\psi] K^\pm$ decay processes by the Belle experiment [1], and confirmed by CDF [2], D0 [3] and BaBar [4]. As the first candidate of an exotic charmonium-like state, it has been studied in numerous experimental analyses over the past two decades. Along with a well-established quantum number $J^{PC} = 1^{++}$ [5], many remarkable features of the $X(3872)$ have been observed, including a mass almost exactly at the $D^{*0} \bar{D}^0$ threshold, an extremely narrow width [6], and an isospin-violating decay pattern [7–9]. For the nature of the $X(3872)$, many theoretical interpretations have been proposed, including a hadronic molecule [10, 11], a compact tetraquark state [12], a conventional charmonium state $\chi_{c1}(2P)$ [13], a mixture of a molecule and an excited charmonium state [14–16] and so on. However, none of these explanations has been universally accepted.

The lineshape of the $X(3872)$ contains essential information, since from its parameters it is possible to extract the pole locations, the effective range of the particle interaction and the scattering length. Here, the pole of a physical state refers to the corresponding sin-

gle pole of the off-shell T-matrix in the complex energy plane, where the amplitude becomes infinite. Recently, the LHCb experiment performed a lineshape study based on a high-statistics $X(3872) \rightarrow \pi^+ \pi^- J/\psi$ data sample, with both Breit-Wigner and Flatté models [17]. However, the lineshapes based on these two models can not be distinguished once the mass resolution is considered. Due to the proximity to the $D^* \bar{D}$ threshold, the lineshape of the $X(3872)$ in the $D^{*0} \bar{D}^0$ channel is significantly distorted, making this channel more sensitive to the behavior of the T-matrix. A study of $X(3872) \rightarrow D^* \bar{D}$ has previously been performed by Belle [18]; however, the off-shell effect of the D^{*0} was not taken into account due to a mass constraint applied to the $D^0 \pi^0$ and $D^0 \gamma$ systems coming from the D^{*0} , which forced the distribution to start from the $D^{*0} \bar{D}^0$ threshold. In the meantime, data samples of both $X(3872) \rightarrow \pi^+ \pi^- J/\psi$ and $X(3872) \rightarrow D^0 \bar{D}^0 \pi^0$ channels were acquired by BESIII [19], allowing a simultaneous fit, taking into account the coupled-channel effect and the width of the D^{*0} , which can improve the $X(3872)$ lineshape measurement.

In this Letter, we present a study of the $X(3872)$

lineshape using e^+e^- annihilation data collected with the BESIII detector at center-of-mass energies ranging from 4.178 to 4.278 GeV, already used in previous $X(3872)$ studies [19]. The total integrated luminosity is 9.0 fb^{-1} [20, 21]. The data samples used have center-of-mass energies around the $Y(4230)$ mass peak, since these energies correspond to a maximum in the $X(3872)$ production cross section. The pole locations of the $X(3872)$ are determined based on a simultaneous fit to the data samples of $X(3872) \rightarrow D^0 \bar{D}^0 \pi^0$ and $X(3872) \rightarrow \pi^+ \pi^- J/\psi$, with the $X(3872)$ produced in the $e^+e^- \rightarrow \gamma X(3872)$ process. Throughout this Letter, the charge conjugations are always included and the notations $D^{*0} \bar{D}^0$ and $D^{*+} D^-$ denote both themselves and their charge conjugations.

The parameterization scheme in this analysis is developed based on the framework described in Ref. [22], taking into account the effects of the D^{*0} width. In this framework, the $X(3872)$ decays into the three-body final state $D^0 \bar{D}^0 \pi^0$ via intermediate $D^{*0} \bar{D}^0$. The differential decay rate is written as

$$\begin{aligned} \frac{d\text{Br}(D^0 \bar{D}^0 \pi^0)}{dE} &= \mathcal{B} \frac{\text{Br}(D^{*0} \rightarrow D^0 \pi^0) \times g \times k_{\text{eff}}(E)}{|D(E)|^2}, \\ \frac{d\text{Br}(\pi^+ \pi^- J/\psi)}{dE} &= \mathcal{B} \frac{\Gamma_{\pi^+ \pi^- J/\psi}}{|D(E)|^2}, \end{aligned} \quad (1)$$

where the denominator is

$$\begin{aligned} D(E) &= E - E_X + \frac{1}{2}g[(\kappa_{\text{eff}}(E) + ik_{\text{eff}}(E)) \\ &\quad + (\kappa_{\text{eff}}^c(E) + ik_{\text{eff}}^c(E))] + \frac{i}{2}\Gamma_0. \end{aligned} \quad (2)$$

In the above equations, all the details of the $X(3872)$ production are assumed to be absorbed in a global constant factor \mathcal{B} , while Br denotes the branching fractions, and g denotes the effective coupling constant of the $X(3872)$ to neutral and charged $D^* \bar{D}$. The energy E (E_X) is measured with respect to the three-body $D^0 \bar{D}^0 \pi^0$ threshold, and is related to the invariant mass of the final states (the mass of the $X(3872)$) by $M_{(X)} = m_{D^0} + m_{\bar{D}^0} + m_{\pi^0} + E_{(X)}$, where m_{D^0} , $m_{\bar{D}^0}$ and m_{π^0} are the masses of D^0 , \bar{D}^0 and π^0 quoted from the Particle Data Group (PDG) [6]. The constant Γ_0 includes the width of all channels except $D^* \bar{D}$, and is comprised of three parts: $\Gamma_0 = \Gamma_{\pi^+ \pi^- J/\psi} + \Gamma_{\text{known}} + \Gamma_{\text{unknown}} = (1 + \beta + \alpha)\Gamma_{\pi^+ \pi^- J/\psi}$. Here, $\Gamma_{\pi^+ \pi^- J/\psi}$, Γ_{known} and Γ_{unknown} are the partial widths of the $\pi^+ \pi^- J/\psi$ channel, the other measured channels ($\gamma J/\psi$, $\gamma \psi(3686)$, $\pi^0 \chi_{c1}$, and $\omega J/\psi$) and the unknown channels, respectively. Due to limited statistics, the ratio $\alpha = \Gamma_{\text{unknown}}/\Gamma_{\pi^+ \pi^- J/\psi}$ is fixed at 8 and the ratio $\beta = \Gamma_{\text{known}}/\Gamma_{\pi^+ \pi^- J/\psi}$ is fixed at 2.8 according to a global analysis of $X(3872)$ decays [23]. The parameterization of the self-energy terms $\kappa_{\text{eff}}^{(c)}(E)$ and $k_{\text{eff}}^{(c)}(E)$ (the superscript c indicates the charged $D^{*+} D^-$) can be found in the supplemental material [24].

The expected numbers of signal events in the two decay channels, $\mu_{D^0 \bar{D}^0 \pi^0}$ and $\mu_{\pi^+ \pi^- J/\psi}$, are related to the

number of produced $e^+e^- \rightarrow \gamma X(3872)$ events, $\mu_{X(3872)}^{\text{prod}}$, as follows:

$$\begin{aligned} \mu_{D^0 \bar{D}^0 \pi^0} &= \epsilon_{D^0 \bar{D}^0 \pi^0} \times R_{D^0 \bar{D}^0 \pi^0} \times \mu_{X(3872)}^{\text{prod}}, \\ \mu_{\pi^+ \pi^- J/\psi} &= \epsilon_{\pi^+ \pi^- J/\psi} \times R_{\pi^+ \pi^- J/\psi} \times \mu_{X(3872)}^{\text{prod}}. \end{aligned} \quad (3)$$

Here, $\epsilon_{D^0 \bar{D}^0 \pi^0}$ ($\epsilon_{\pi^+ \pi^- J/\psi}$) represents the efficiency of the $D^0 \bar{D}^0 \pi^0$ ($\pi^+ \pi^- J/\psi$) channel multiplied by the branching fractions of the decay chains $D^0 \rightarrow K^- \pi^+$, $K^- \pi^+ \pi^0$, $K^- 2\pi^+ \pi^-$, $\pi^0 \rightarrow \gamma \gamma$ ($J/\psi \rightarrow e^+e^-$, $\mu^+ \mu^-$), i.e. 1.31×10^{-3} (3.78×10^{-2}) according to Refs. [6, 9, 19], while $R_{D^0 \bar{D}^0 \pi^0}$ ($R_{\pi^+ \pi^- J/\psi}$) represents the branching fraction of $X(3872) \rightarrow D^0 \bar{D}^0 \pi^0$ ($X(3872) \rightarrow \pi^+ \pi^- J/\psi$) derived from the lineshape analysis.

The mass resolutions of the two channels are studied based on Monte Carlo (MC) simulation. The MC samples are generated with zero $X(3872)$ width and a series of mass values in the range of interest. For the $D^0 \bar{D}^0 \pi^0$ channel, the mass resolution is modeled as a Gaussian function, with a constant mean and a linear mass-dependent width. For the $\pi^+ \pi^- J/\psi$ channel, the mass resolution is modeled by a Gaussian function, whose parameters are determined by the control sample $e^+e^- \rightarrow \gamma_{\text{ISR}}[\psi(2S) \rightarrow \pi^+ \pi^- J/\psi]$ and calculated at 3.872 GeV. The values of mass shift and resolution can be found in the supplemental material [24].

TABLE I. Summary of the $X(3872)$ lineshape fit parameters.

Parameter	Symbol	Value
Coupling constant	g	fit
Partial width of $\pi^+ \pi^- J/\psi$	$\Gamma_{\pi^+ \pi^- J/\psi}$	fit
Physical mass of $X(3872)$	M_X	fit
Mass of D^{*0}	-	2.00685 GeV
Width of D^{*0}	-	55.9 keV
Width of $D^{*\pm}$	-	83.4 keV
$\Gamma_{\text{known}}/\Gamma_{\pi^+ \pi^- J/\psi}$	β	2.8
$\Gamma_{\text{unknown}}/\Gamma_{\pi^+ \pi^- J/\psi}$	α	8
Total number of $X(3872)$	$\mu_{X(3872)}^{\text{prod}}$	fit
Efficiency correction ^a	$\epsilon_{D^0 \bar{D}^0 \pi^0}$	1.31×10^{-3} [19]
	$\epsilon_{\pi^+ \pi^- J/\psi}$	3.78×10^{-2} [9]

^a Multiplied with branching fractions of daughter particles' decay.

An unbinned maximum likelihood fit is performed simultaneously to the invariant mass distributions of $M(\pi^+ \pi^- J/\psi)$ and $M(D^0 \bar{D}^0 \pi^0)$, whose parameters are summarized in Table I. In the fit, to improve the mass resolution, the variable $M(\pi^+ \pi^- J/\psi) = M(\pi^+ \pi^- l^+ l^-) - M(l^+ l^-) + m_{J/\psi}$ is used, where $l^+ l^-$ stands for $e^+ e^-$ or $\mu^+ \mu^-$, and $m_{J/\psi}$ is the J/ψ mass [6]. The background shapes for the $D^0 \bar{D}^0 \pi^0$ and $\pi^+ \pi^- J/\psi$ channels are described, respectively, by an ARGUS function [25] with threshold parameters fixed at the $D^0 \bar{D}^0 \pi^0$ nominal mass, and by a second order Chebyshev function. The obtained lineshape parameters are shown in Table II, and

the number of produced $X(3872)$ is determined to be $\mu_{X(3872)}^{\text{prod}} = (9.8 \pm 3.9) \times 10^4$. Here, the floating parameter in the fit is $\Gamma_{\pi^+\pi^-J/\psi}$ and its value is transformed into $\Gamma_0 = (1 + \alpha + \beta)\Gamma_{\pi^+\pi^-J/\psi}$ throughout the letter for convenience. The fit result is shown in Fig. 1(a) and 1(b), and the obtained $X(3872)$ lineshape, adding all channels together, is shown in Fig. 1(c), with a full width at the half maximum (FWHM) of 0.44 MeV.

TABLE II. The fit results of the lineshape parameters and the correlation matrix.

Parameters	g	Γ_0 (MeV)	M_X (MeV)
Fit results	0.16 ± 0.10	2.67 ± 1.77	3871.63 ± 0.13
g	1.00	0.89	-0.60
Γ_0		1.00	-0.29
M_X			1.00

The systematic uncertainties are estimated as follows.

The uncertainty caused by the choice of the ratios $\alpha = \Gamma_{\text{unknown}}/\Gamma_{\pi^+\pi^-J/\psi}$ and $\beta = \Gamma_{\text{known}}/\Gamma_{\pi^+\pi^-J/\psi}$ is evaluated by varying $\alpha + \beta$ in the range (4.2, 21.8), according to Ref. [23].

The D^{*0} nominal width is quoted from an evaluation based on heavy quark symmetry [26]. The corresponding uncertainty is estimated by varying the value in the range (50, 70) keV in the lineshape models, where the range is determined according to various calculations of the D^{*0} width (55.9 keV in Ref. [26], 53.7 keV in Ref. [27] and 68 keV in Ref. [28]).

The relative uncertainty from the efficiency ratios of the $D^0\bar{D}^0\pi^0$ and $\pi^+\pi^-J/\psi$ decays is assigned to be 10% according to the uncorrelated uncertainties in Ref. [9, 19], and is propagated to the lineshape parameters by changing the corresponding values in Eq. (3).

The discrepancy in the $D^0\bar{D}^0\pi^0$ mass resolution between MC simulation and data (referred to as *Resolution* in Table III) is studied using the control sample $e^+e^- \rightarrow [D^{*0} \rightarrow D^0\pi^0]\bar{D}^0$. The discrepancy is parameterized as a Gaussian function and extracted from the distribution of $M_{\text{control}} = |2p_D + p_{\pi^0}|$, where p_{π^0} and p_D denote the four-momentum of the π^0 and of the D^0 decaying from D^{*0} , respectively. The obtained Gaussian function is convoluted additionally with the lineshape for uncertainty evaluation. For the $\pi^+\pi^-J/\psi$ channel, since the MC invariant mass has been modeled to data by using the control sample, the related systematic uncertainty is treated as negligible.

For the background models (referred as *Background* in Table III), the uncertainty is evaluated by changing the ARGUS function to a third order polynomial, and changing the order of the Chebyshev function from second to third, respectively.

The uncertainty of the D^0 mass, 50 keV [6], is propagated to the lineshape parameters by changing the D^0 mass by plus or minus 50 keV in the analysis procedure.

The center-of-mass energies of the e^+e^- collisions for

the datasets used in this work are obtained from a measurement of di-muon events, as described in Ref. [29]. A common uncertainty of 0.8 MeV for each dataset is adopted, and it is propagated to the lineshape parameters by changing the values of the center-of-mass energies accordingly when applying the kinematic constraints in the event selection.

The uncertainties caused by MC simulation configurations (referred as *Simulation* in Table III), including the input cross sections and the generator models used in the decay chains, are evaluated as follows. For the input cross sections of $e^+e^- \rightarrow \gamma X(3872)$, the measured cross sections of Ref. [9] are used, instead of using the $Y(4230)$ lineshape quoted from the PDG; for the $\gamma X(3872)$ angular distribution, it is changed from an E1 transition to a pure S-wave; the $\pi^+\pi^-$ pair in the $\pi^+\pi^-J/\psi$ channel is assumed to come from a ρ^0 decay, and for the $\rho J/\psi$ angular distribution from $X(3872)$ the partial wave analysis result of Ref. [5] is adopted, instead of the original S-wave assumption.

For each of the above mentioned sources of systematic uncertainties, the largest differences caused by varying the values or modifying the inputs with respect to the nominal values are taken as systematic uncertainties, and are treated as independent. The systematic uncertainties of the lineshape parameters are summarized in Table III, where the last row is obtained by summing each term in quadrature.

TABLE III. Systematic uncertainties of the lineshape parameters.

Source	g	Γ_0 (MeV)	M_X (MeV)
α	+1.08 - 0.10	+6.54 - 0.65	+0.05 - 0.04
$\Gamma_{D^{*0}}$	-	+0.05 - 0.07	-
Efficiency	+0.05 - 0.03	+0.35 - 0.24	-
Resolution	-	± 0.02	-
Background	+0.05	+0.51 - 0.24	± 0.01
$M(D^0)$	-	+0.11 - 0.09	± 0.03
E_{cms}	+0.29	+4.57	-0.01
Simulation	± 0.02	± 0.26	± 0.01
Sum	+1.12 - 0.11	+8.01 - 0.82	+0.06 - 0.05

The analytic structure of the amplitude and the corresponding pole locations are studied by extending the energy E from the real axis to the whole complex plane. According to the simplified form in the supplemental material [24], there are two Riemann sheets with respect to the $D^{*0}\bar{D}^0$ threshold, defined by the sign of the $D^{*0}\bar{D}^0$ self-energy term:

$$\begin{aligned}
 \text{sheet I: } & -g\sqrt{-2\left(E - E_R + \frac{i\Gamma_{D^{*0}}}{2}\right) + i\Gamma_0}, \\
 \text{sheet II: } & +g\sqrt{-2\left(E - E_R + \frac{i\Gamma_{D^{*0}}}{2}\right) + i\Gamma_0}.
 \end{aligned} \tag{4}$$

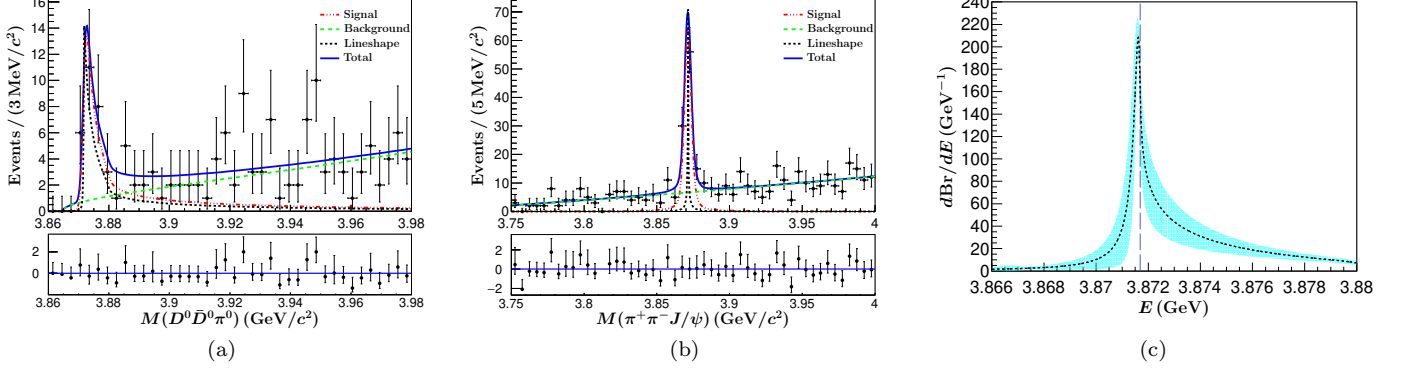


FIG. 1. Distributions of (a) $D^0 \bar{D}^0 \pi^0$ and (b) $\pi^+ \pi^- J/\psi$ invariant mass. The black dots with error bars are the data from Ref. [19]; the blue continuous lines are the probability density functions at the best estimation; the red dotted lines are the signal shapes; the green dashed lines are the background shapes; and the black dashed lines represent the lineshape without the mass resolution considered, normalized to the signal height for comparison. (c) The $X(3872)$ lineshape at the best estimation. The cyan shaded band indicates the statistical uncertainty and the vertical dashed line indicates the position of the $D^{*0} \bar{D}^0$ threshold.

The numerical results on the pole locations are obtained using a complex roots finding algorithm [30]. The pole locations are visualized by plotting the phase of the amplitude, as shown in Fig. 2, where the phase is indefinite around the poles and discontinuous across the branch cut. With the nominal lineshape parameters, two poles are found: one is on sheet I, denoted as E_{I} , while the other is on sheet II, denoted as E_{II} . In Fig. 2, when scaling down Γ_0 to 0, all channels except $D^* \bar{D}$ switch off, showing that the location of E_{I} is much closer to the $D^{*0} \bar{D}^0$ threshold than E_{II} .

The pole locations on the k -plane are also investigated. The momentum k is defined by $k = \sqrt{2\mu_p} \sqrt{E - E_R + \frac{i\Gamma_{D^{*0}}}{2}}$, where μ_p is the two-body reduced mass, and $D(E)$ in Eq. (2) can be rewritten as a function of k :

$$D(k) = \frac{1}{a} - ik + \frac{r_e}{2} k^2 + \mathcal{O}(k^3), \quad (5)$$

where a is the scattering length and r_e is the effective range [31]. The high order term occurs due to the presence of charged channels. By doing so, the poles can be displayed in one plane, as shown in Fig. 2(c). The pole location on the upper half plane is $k^+ = (-12.6 + 12.3i)$ MeV, and that on the lower half plane is $k^- = (14.1 - 115.3i)$ MeV.

The statistical uncertainties of the pole locations, propagated from the lineshape parameters g , Γ_0 , and M_X , are obtained by sampling the lineshape parameters according to their covariance matrix. Here, since the uncertainties are large, g and $\Gamma_{\pi^+ \pi^- J/\psi}$ could become negative in the 3σ confidence region, which exceeds the physical boundary. The events with negative g or $\Gamma_{\pi^+ \pi^- J/\psi}$ are dropped when calculating the statistical uncertainties of the pole locations (and other related parameters, as described as follows). The system-

atic uncertainties are obtained using the same treatment as that of the lineshape parameters. The detailed information of statistical and systematic uncertainties can be found in the supplemental material [24]. The pole locations including uncertainties are determined to be $E_{\text{I}} = (7.04 \pm 0.15_{-0.08}^{+0.07}) + (-0.19 \pm 0.08_{-0.19}^{+0.14}) i$ MeV and $E_{\text{II}} = (0.26 \pm 5.74_{-38.32}^{+5.14}) + (-1.71 \pm 0.90_{-1.96}^{+0.60}) i$ MeV on the Riemann sheets, and $k^+ = (-12.6 \pm 5.5_{-6.2}^{+6.6}) + (12.3 \pm 6.8_{-6.4}^{+6.0}) i$ MeV and $k^- = (14.1 \pm 5.8_{-2.1}^{+5.3}) + (-115.3 \pm 44.6_{-192.8}^{+52.7}) i$ MeV on the k -plane.

The relative ratio of the branching fractions of $\pi^+ \pi^- J/\psi$ and $D^0 \bar{D}^0 \pi^0$ is determined to be $\frac{\Gamma(X(3872) \rightarrow \pi^+ \pi^- J/\psi)}{\Gamma(X(3872) \rightarrow D^0 \bar{D}^0 \pi^0)} = 0.05 \pm 0.01_{-0.02}^{+0.01}$, which is consistent with the global fit result 0.08 ± 0.04 [23] and 2020 BESIII result 0.08 ± 0.02 [19] within 1σ , but lower than the value used as a Gaussian constraint in LHCb's work 0.11 ± 0.03 [17]. Compared to the previous result in Ref. [19], the ratio is larger mainly due to the inclusion of the $D^{*+} D^-$ term in the model, which extends the tail of the lineshape in the $D^0 \bar{D}^0 \pi^0$ channel and results in a larger signal yield.

We have estimated the effective range expansion (ERE) parameters, i.e. the scattering length a and the effective range r_e in Eq. (5). We consider a simplified case, according to the discussion in Ref. [32], by setting Γ_0 and Γ_{D^*} to be 0. The amplitude is reduced to a single channel, $D^* \bar{D}$, and the D^* is treated as a stable particle. After the simplification, the ERE parameters are determined to be $a = (-16.5_{-27.6}^{+7.0} \quad +5.6_{-27.7})$ fm and $r_e = (-4.1_{-3.3}^{+0.9} \quad +2.8_{-4.4})$ fm.

Based on the obtained results, we can do a comparison between the $X(3872)$ and the deuteron. The ERE parameters are related to the field renormalization constant Z by:

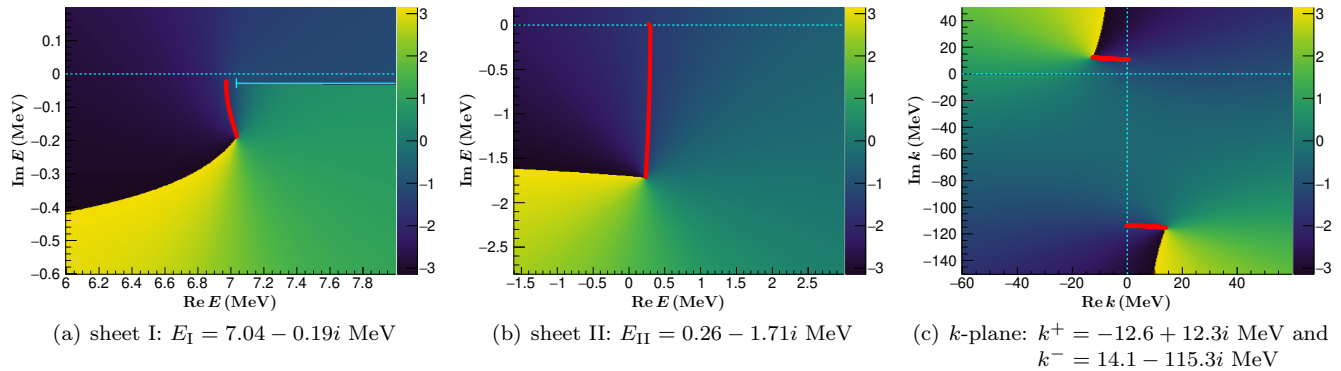


FIG. 2. The phase of the amplitude on (a) sheet I and (b) sheet II with respect to complex energy. The solid cyan line starting from the point $7.033 - 0.027i$ MeV is the branch cut, the dashed cyan line is the real axis and the red trajectory approaching the real axis is obtained by continuously decreasing Γ_0 to 0. (c) The phase of the amplitude with respect to k . The upper (lower) half plane corresponds to sheet I (sheet II).

$$a = -\frac{2(1-Z)}{(2-Z)} \frac{1}{\gamma} + \mathcal{O}(\beta^{-1}), \quad (6)$$

$$r_e = -\frac{Z}{1-Z} \frac{1}{\gamma} + \mathcal{O}(\beta^{-1}). \quad (7)$$

where $\gamma = \sqrt{2\mu_p E_B}$, with E_B the binding energy; the scale β measures the momentum scale of the binding interaction, which cannot be calculated without knowing the details of the interaction, but can be estimated to be of the order of the pion mass m_π for both neutron-proton and $D^*\bar{D}$ interactions, i.e. $1/\beta \sim 1/m_\pi \simeq 1.4$ fm.

In the limit of $Z \rightarrow 0$, the effective range should be positive and dominated by the range correction [32–35]. It was found that this case is compatible with the measured ERE parameters of the deuteron, which is known to be a predominantly molecular state [33]. However, in the case of the $X(3872)$, we see that a negative effective range can fit the data well, which is different from the deuteron case (+1.75 fm) and also suggests an elementary component in the $X(3872)$ [32]. Given that the range correction is less important in the case of the $X(3872)$, one can solve Eqs. (6) and (7) for Z by neglecting $\mathcal{O}(\beta^{-1})$, and obtain $Z = 0.18$. However, in the case of the deuteron, it would be impossible to solve Eqs. (6) and (7) for Z in a model independent way since the range correction term is non-negligible for r_e . Despite this, using the generalized compositeness \tilde{X}_A proposed in Ref. [35], we find both the $X(3872)$ and the deuteron have similar compositeness. Nevertheless, there are still large uncertainties in the ERE parameters, which prevent us from drawing strong conclusions on the nature of the $X(3872)$. More statistics would be helpful.

In summary, we measure the lineshape of the $X(3872)$ by performing a simultaneous fit to the decay channels $D^0\bar{D}^0\pi^0$ and $\pi^+\pi^-J/\psi$. The lineshape parameters are determined to be $g = 0.16 \pm 0.10^{+1.12}_{-0.11}$, $\Gamma_0 = (2.67 \pm 1.77^{+8.01}_{-0.82})$ MeV and $M_X = (3871.63 \pm 0.13^{+0.06}_{-0.05})$ MeV,

where the first and second uncertainties are statistical and systematical, respectively. The FWHM of the lineshape is determined to be $(0.44^{+0.13}_{-0.35} \text{ } ^{+0.38}_{-0.25})$ MeV.

The BESIII Collaboration thanks the staff of BEPCII and the IHEP computing center for their strong support. This work is supported in part by National Key R&D Program of China under Contracts Nos. 2020YFA0406300, 2020YFA0406400; National Natural Science Foundation of China (NSFC) under Contracts Nos. 11635010, 11735014, 11835012, 11935015, 11935016, 11935018, 11961141012, 12022510, 12025502, 12035009, 12035013, 12061131003, 12192260, 12192261, 12192262, 12192263, 12192264, 12192265, 12221005, 12225509, 12235017; the Chinese Academy of Sciences (CAS) Large-Scale Scientific Facility Program; the CAS Center for Excellence in Particle Physics (CCEPP); Joint Large-Scale Scientific Facility Funds of the NSFC and CAS under Contract No. U1832207; CAS Key Research Program of Frontier Sciences under Contracts Nos. QYZDJ-SSW-SLH003, QYZDJ-SSW-SLH040; 100 Talents Program of CAS; The Institute of Nuclear and Particle Physics (INPAC) and Shanghai Key Laboratory for Particle Physics and Cosmology; ERC under Contract No. 758462; European Union’s Horizon 2020 research and innovation programme under Marie Skłodowska-Curie grant agreement under Contract No. 894790; German Research Foundation DFG under Contracts Nos. 443159800, 455635585, Collaborative Research Center CRC 1044, FOR5327, GRK 2149; Istituto Nazionale di Fisica Nucleare, Italy; Ministry of Development of Turkey under Contract No. DPT2006K-120470; National Research Foundation of Korea under Contract No. NRF-2022R1A2C1092335; National Science and Technology fund of Mongolia; National Science Research and Innovation Fund (NSRF) via the Program Management Unit for Human Resources & Institutional Development, Research and Innovation of Thailand under Contract No. B16F640076; Polish National Science Centre under Contract No. 2019/35/O/ST2/02907; The Swedish Research

-
- [1] S. K. Choi *et al.* [Belle Collaboration], *Phys. Rev. Lett.* **91**, 262001 (2003).
- [2] D. Acosta *et al.* [CDF Collaboration], *Phys. Rev. Lett.* **93**, 072001 (2004).
- [3] V. M. Abazov *et al.* [D0 Collaboration], *Phys. Rev. Lett.* **93**, 162002 (2004).
- [4] B. Aubert *et al.* [BaBar Collaboration], *Phys. Rev. D* **71**, 071103 (2005).
- [5] R. Aaij *et al.* [LHCb Collaboration], *Phys. Rev. D* **92**, 011102 (2015).
- [6] R. L. Workman *et al.* [Particle Data Group], *PTEP* **2022**, 083C01 (2022).
- [7] K. Abe *et al.* [Belle Collaboration], [hep-ex/0505037](#) [hep-ex].
- [8] P. del Amo Sanchez *et al.* [BaBar Collaboration], *Phys. Rev. D* **82**, 011101 (2010).
- [9] M. Ablikim *et al.* [BESIII Collaboration], *Phys. Rev. Lett.* **122**, 232002 (2019).
- [10] E. S. Swanson, *Phys. Lett. B* **588**, 189 (2004).
- [11] L. Zhao, L. Ma, and S.-L. Zhu, *Phys. Rev. D* **89**, 094026 (2014).
- [12] L. Maiani, F. Piccinini, A. D. Polosa, and V. Riquer, *Phys. Rev. D* **71**, 014028 (2005).
- [13] N. N. Achasov and E. V. Rogozina, *Mod. Phys. Lett. A* **30**, 1550181 (2015).
- [14] M. Suzuki, *Phys. Rev. D* **72**, 114013 (2005).
- [15] Y. S. Kalashnikova, *Phys. Rev. D* **72**, 034010 (2005).
- [16] M. Takizawa and S. Takeuchi, *PTEP* **2013**, 093D01 (2013).
- [17] R. Aaij *et al.* [LHCb Collaboration], *Phys. Rev. D* **102**, 092005 (2020).
- [18] T. Aushev *et al.* [Belle Collaboration], *Phys. Rev. D* **81**, 031103 (2010).
- [19] M. Ablikim *et al.* [BESIII Collaboration], *Phys. Rev. Lett.* **124**, 242001 (2020).
- [20] M. Ablikim *et al.* [BESIII Collaboration], *Chinese Physics C* **39**, 093001 (2015).
- [21] M. Ablikim *et al.* [BESIII Collaboration], *Chinese Physics C* **46**, 113002 (2022).
- [22] C. Hanhart, Y. S. Kalashnikova, and A. V. Nefediev, *Phys. Rev. D* **81**, 094028 (2010).
- [23] C. Li and C.-Z. Yuan, *Phys. Rev. D* **100**, 094003 (2019).
- [24] See Supplemental Material at [the link to be inserted by the editor](#) for details about lineshape parameterization, the determination of the mass resolution and the uncertainties of the pole location.
- [25] H. Albrecht *et al.*, *Physics Letters B* **241**, 278 (1990).
- [26] J. L. Rosner, *Phys. Rev. D* **88**, 034034 (2013).
- [27] M.-L. Du, V. Baru, X.-K. Dong, A. Filin, F.-K. Guo, C. Hanhart, A. Nefediev, J. Nieves, and Q. Wang, *Phys. Rev. D* **105**, 014024 (2022).
- [28] C. Hanhart, Y. S. Kalashnikova, A. E. Kudryavtsev, and A. V. Nefediev, *Phys. Rev. D* **76**, 034007 (2007).
- [29] M. Ablikim *et al.* [BESIII Collaboration], *Chin. Phys. C* **40**, 063001 (2016).
- [30] P. Kowalczyk, *IEEE Transactions on Antennas and Propagation* **66**, 7198 (2018).
- [31] T. Hyodo, *Phys. Rev. Lett.* **111**, 132002 (2013).
- [32] A. Esposito, L. Maiani, A. Pilloni, A. D. Polosa, and V. Riquer, *Phys. Rev. D* **105**, L031503 (2022).
- [33] S. Weinberg, *Phys. Rev.* **137**, B672 (1965).
- [34] V. Baru, X.-K. Dong, M.-L. Du, A. Filin, F.-K. Guo, C. Hanhart, A. Nefediev, J. Nieves, and Q. Wang, *Physics Letters B* **833**, 137290 (2022).
- [35] I. Matuschek, V. Baru, F.-K. Guo, and C. Hanhart, *Eur. Phys. J. A* **57**, 101 (2021), [arXiv:2007.05329](#) [hep-ph].

Supplemental material

I. SELF-ENERGY TERMS PARAMETERIZATION

The parameterizations of the self-energy terms $\kappa_{\text{eff}}(E)$ and $k_{\text{eff}}(E)$ corresponding to the coupling with the $D^{*0}\bar{D}^0$ channel are the following:

$$\begin{aligned} k_{\text{eff}}(E) &= \sqrt{\mu_p} \sqrt{\sqrt{(E - E_R)^2 + \Gamma_{D^{*0}}^2/4} + E - E_R}, \\ \kappa_{\text{eff}}(E) &= -\sqrt{\mu_p} \sqrt{\sqrt{(E - E_R)^2 + \Gamma_{D^{*0}}^2/4} - E + E_R} \\ &\quad + \sqrt{\mu_p} \sqrt{\sqrt{(E_X - E_R)^2 + \Gamma_{D^{*0}, X}^2/4} - E_X + E_R}. \end{aligned} \quad (1)$$

The energy-dependent width $\Gamma_{D^{*0}} = \Gamma_{D^{*0}}(E)$ is expressed as:

$$\Gamma_{D^{*0}}(E) = \Gamma_{D^{*0}}^0 \times \left(\text{Br}(D^{*0} \rightarrow D^0\pi^0) \times \left(\frac{E}{E_R}\right)^{3/2} + \text{Br}(D^{*0} \rightarrow \gamma D^0) \right), \quad (2)$$

and $\Gamma_{D^{*0}, X} = \Gamma_{D^{*0}}(E_X)$, where $\Gamma_{D^{*0}}^0 = 55.9$ keV is the nominal width of D^{*0} , $E_R = m_{D^{*0}} - m_{D^0} - m_{\pi^0}$, and the two-body reduced mass is $\mu_p = \frac{m_{D^{*0}}m_{\bar{D}^0}}{m_{D^{*0}}+m_{\bar{D}^0}}$.

The terms $\kappa_{\text{eff}}^c(E)$ and $k_{\text{eff}}^c(E)$ corresponding to the charged $D^{*+}D^-$ are obtained by the following replacements in equations (1): $\mu_p \rightarrow \mu_p^c$, $\Gamma_{D^{*0}, (X)}(E) \rightarrow \Gamma_{D^{*+}, (X)}(E)$, $E_R \rightarrow E_R^c$, where the width of the D^{*+} is

$$\Gamma_{D^{*+}}(E) = \Gamma_{D^{*+}}^0 \times \left(\text{Br}(D^{*+} \rightarrow D^+\pi^0) \times \left(\frac{E_{D^+D^-\pi^0}}{E_R^c}\right)^{3/2} + \text{Br}(D^{*+} \rightarrow D^0\pi^+) \times \left(\frac{E_{D^0D^-\pi^+}}{E_R^c}\right)^{3/2} + \text{Br}(D^{*+} \rightarrow D^+\gamma) \right), \quad (3)$$

and $\Gamma_{D^{*+}, X} = \Gamma_{D^{*+}}(E_X)$, where $\Gamma_{D^{*+}}^0 = 83.4$ keV is the nominal width of the D^{*+} , $E_R^c = m_{D^{*+}} + m_{D^-} - (m_{D^0} + m_{\bar{D}^0} + m_{\pi^0})$, $\mu_p^c = (m_{D^{*+}}m_{D^-})/(m_{D^{*+}} + m_{D^-})$, $E_{D^+D^-\pi^0} = M - m_{D^+} - m_{D^-} - m_{\pi^0}$, and $E_{D^0D^-\pi^+} = M - m_{D^0} - m_{D^-} - m_{\pi^+}$.

For convenience, for the pole search the self-energy terms can be simplified using the following identity:

$$\sqrt{\sqrt{(E - E_R)^2 + \frac{\Gamma_{D^{*0}}^2}{4}} - E + E_R} - i\sqrt{\sqrt{(E - E_R)^2 + \frac{\Gamma_{D^{*0}}^2}{4}} + E - E_R} = \sqrt{-2\left(E - E_R + \frac{i\Gamma_{D^{*0}}}{2}\right)}, \quad (4)$$

and the self-energy terms become

$$\kappa_{\text{eff}} + ik_{\text{eff}} = \sqrt{\mu_p} * \left(-\sqrt{-2\left(E - E_R + \frac{i\Gamma_{D^{*0}}}{2}\right)} + \sqrt{\sqrt{(E_X - E_R)^2 + \frac{\Gamma_{D^{*0}, X}^2}{4}} - E_X + E_R} \right). \quad (5)$$

II. DETERMINATION OF THE MASS RESOLUTION

To determine the mass resolution, MC samples are generated. For the $D^0\bar{D}^0\pi^0$ channel, samples of $e^+e^- \rightarrow \gamma[X(3872) \rightarrow D^0\bar{D}^0\pi^0]$ are generated with zero $X(3872)$ width and values of mass ranging from the threshold to 30 MeV above. For the $\pi^+\pi^-J/\psi$ channel, samples of $e^+e^- \rightarrow \gamma[X(3872) \rightarrow \pi^+\pi^-J/\psi]$ are generated with zero $X(3872)$ width and values of mass ranging from 3.686 GeV to 3.872 GeV. The MC simulation results are shown in Fig. 1 and 2.

III. SUMMARY OF THE STATISTICAL AND SYSTEMATIC UNCERTAINTIES ON THE POLE LOCATIONS

The confidence regions of the pole locations are shown in Fig. 3, and the covariant matrix of the pole locations are shown in Table I and II. The systematic uncertainties are summarized in Table III and IV.

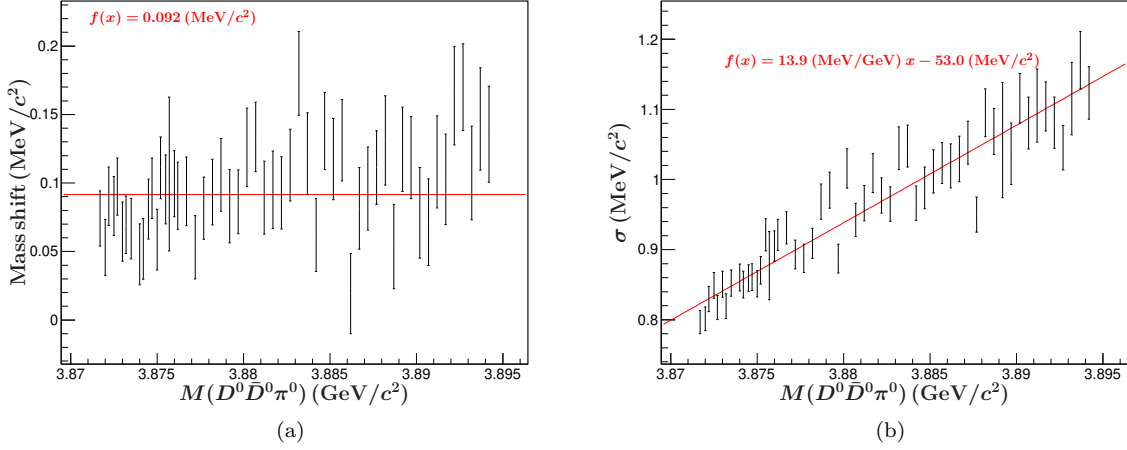


FIG. 1. The (a) mass shift and (b) mass resolution of $D^0 \bar{D}^0 \pi^0$. The red lines are the fit results.

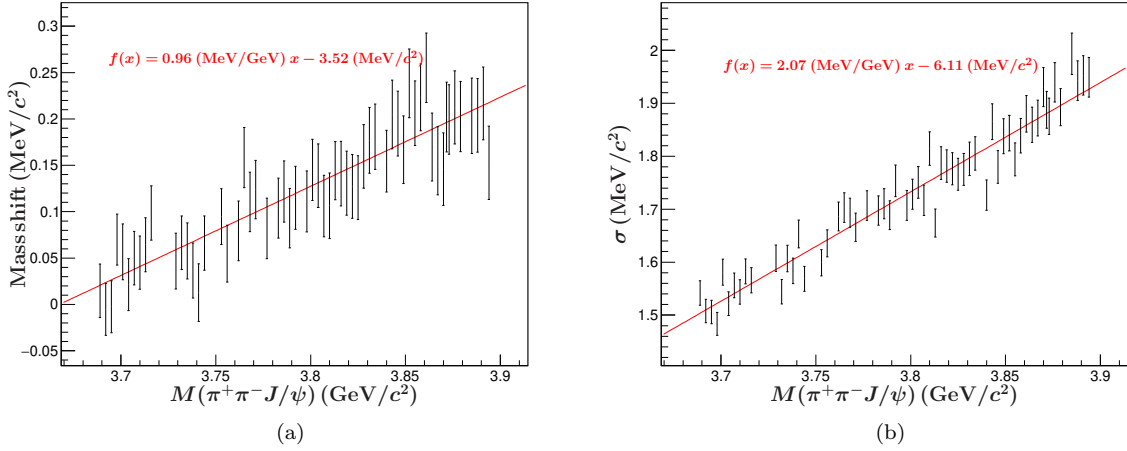


FIG. 2. The MC simulation result of the energy dependence of (a) the mass shift and (b) the resolution. The red lines are the fit results.

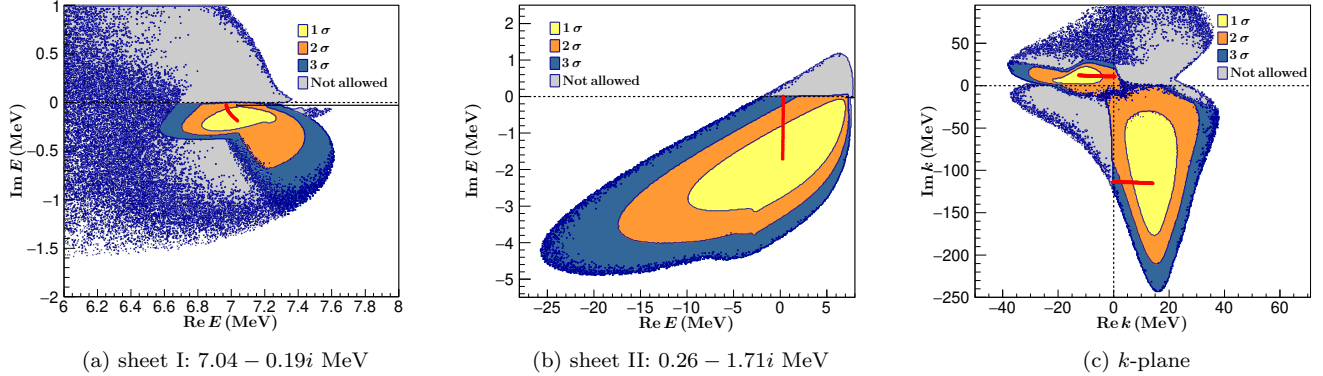


FIG. 3. Confidence regions of the pole position on (a) sheet I and (b) sheet II. Only the statistical uncertainty is shown. The gray region labeled “Not allowed” indicates the region where g or Γ_0 is negative. (c) Confidence region of the pole positions on the k -plane.

TABLE I. The covariance matrix of the locations of the two poles on the two Riemann sheets.

	Re[E_I] (MeV)	Im[E_I] (MeV)	Re[E_{II}] (MeV)	Im[E_{II}] (MeV)
Re[E_I]	0.02	-	0.53	-0.01
Im[E_I]		0.01	0.22	0.03
Re[E_{II}]			32.96	3.79
Im[E_{II}]				0.82

TABLE II. The covariance matrix of the locations of the two poles on the k -plane.

	Re[k^+] (MeV)	Im[k^+] (MeV)	Re[k^-] (MeV)	Im[k^-] (MeV)
Re[k^+]	33.4	16.7	-31.4	-53.6
Im[k^+]		46.3	-14.3	-190.3
Re[k^-]			33.8	8.3
Im[k^-]				1986.3

TABLE III. The upper and lower uncertainties on the pole locations on the Riemann sheets.

Source	Re[E_I] (MeV)	Im[E_I] (MeV)	Re[E_{II}] (MeV)	Im[E_{II}] (MeV)
α	± 0.01	+0.12 - 0.18	+4.74 - 34.20	+0.54 - 0.76
$\Gamma_{D^{*0}}$	± 0.01	± 0.01	+0.23 - 0.20	± 0.03
Efficiency	+0.01	± 0.02	+1.55 - 2.41	+0.13 - 0.18
Resolution	-	-	± 0.08	± 0.01
Background	± 0.02	+0.01	+0.15 - 3.02	- 0.26
$M(D^0)$	± 0.06	± 0.03	+0.34 - 0.16	+0.12 - 0.11
E_{cms}	- 0.03	- 0.06	- 16.79	- 1.77
Simulation	± 0.01	± 0.01	± 1.15	± 0.18
Sum	+0.07 - 0.08	+0.14 - 0.19	+5.14 - 38.32	+0.60 - 1.96

TABLE IV. The upper and lower uncertainties on the pole locations on the k -plane.

Source	Re[k^+] (MeV)	Im[k^+] (MeV)	Re[k^-] (MeV)	Im[k^-] (MeV)
α	+5.9 - 6.0	+5.6 - 5.9	+4.9 - 1.6	+49.8 - 162.5
$\Gamma_{D^{*0}}$	- 0.2	+0.7 - 0.5	- 0.1	+2.0 - 1.7
Efficiency	± 1.0	+0.6 - 0.7	+0.6 - 0.7	+13.7 - 18.6
Resolution	-	-	-	± 0.7
Background	± 1.0	+0.5 - 0.6	+0.5 - 1.0	+1.1 - 24.3
$M(D^0)$	+0.6 - 0.7	+1.7 - 1.9	+0.8 - 0.7	+2.6 - 1.0
E_{cms}	+2.7	+0.2	+1.5	- 98.7
Simulation	± 0.3	± 0.8	± 0.4	± 9.9
Sum	+6.6 - 6.2	+6.0 - 6.4	+5.3 - 2.1	+52.7 - 192.8